Acta Astronautica 132 (2017) 221–229

Contents lists available at ScienceDirect

Acta Astronautica

journal homepage: www.elsevier.com/locate/actaastro

Mars atmospheric entry guidance for reference trajectory tracking based on robust nonlinear compound controller

Juan Dai[a,c,d], Ai Gao[a,c,d,*], Yuanqing Xia[b,c,d]

[a] School of Aerospace Engineering, Beijing Institute of Technology, Beijing 100081, China
[b] School of Automation, Beijing Institute of Technology, Beijing, 100081 China
[c] Key Laboratory of Dynamics and Control of Flight Vehicle, Ministry of Education, Beijing, 100081, China
[d] Key Laboratory of Autonomous Navigation and Control for Deep Space Exploration, Ministry of Industry and Information Technology, China

ARTICLE INFO

Keywords:
Trajectory Tracking
Terminal sliding mode control
Second-order differentiator

ABSTRACT

A robust entry guidance law based on terminal sliding mode and second-order differentiator is designed for trajectory tracking in this paper. The bank angle is regarded as the control variable. A novel nonlinear compound controller is designed to make the system with the trajectory-tracking error and its rate as states be input-to-state stable (ISS) with respect to uncertainties. The terminal sliding mode controller is designed to the problem of entry guidance by using the second-order differentiator to estimate the total disturbances. The proposed nonlinear compound control law by employing the second-order differentiator and the terminal sliding mode controller, provide robustness, higher control precision. Also, simulation results are presented to illustrate the effectiveness of the control strategy.

1. Introduction

Although further improvements in approach navigation will reduce the landing ellipse, it is clear that closed-loop entry guidance will be necessary to achieve landing accuracy on the order of 10 km from a designated target. Several hundreds of kilometers may be covered by an Mars entry vehicle before it lands, while a few tens of kilometers are covered during descent, and usually there is the least possible lateral motion during landing. This means that much of the vehicles landing precision will first and foremost be affected by the state dispersion accumulated during the entry phase, with only small remaining errors that are recoverable during the descent and landing phases(see [1–5]).

For the entry phase of low Lift-to-Drag ratio vehicles, any closed loop guidance system relies on the bank angle to provide active trajectory control. Therefore, a bank angle program must be determined and actively implemented to achieve the desired targeting performances. Generally, schemes for atmospheric entry guidance are divided into major categories, i.e., a) reference trajectory tracking methods and b) predictive trajectory planning methods(see [6–10]).

Recent years, there are some researches on control designs for Mars lander with highly nonlinear characteristics using nonlinear control techniques(see [11–14]). Some of the research results have been achieved in the research of the atmospheric entry guidance and control method of the Mars Lander (see [9,10,15–20]). In [15], a continuous finite time sliding mode controller is designed for the trajectory tracking control of the Martian atmosphere. Non singular terminal sliding mode and finite time control law based on the super screw algorithm. It is realized that the tracking error can converge to zero in finite time. In [20], a multi sliding mode surface navigation method is proposed to track the reference trajectory. But the algorithm does not consider the uncertain disturbance. In the case of multiple constraints, the proposed method is used to solve the problem of trajectory tracking control of the whole state by using the Legendre spectral transform in [21]. In addition to track a reference trajectory of ideas, most of the resistance to tracking navigation method is need to drag velocity, which for Martian atmospheric entry section of the lander, under the real situation is hard to measure precisely [9,10]. In addition, the most effective way to improve the accuracy of the landing point in the complex Martian atmosphere is to ensure that the Mars Lander runs on a predetermined reference trajectory throughout the atmosphere [22]. Then, the Mars Lander if Mars in the complex atmospheric environment, accurate tracking of preset atmospheric entry trajectory for Mars mission critical guidance (see [23,24,15]). Therefore, this paper considers the high speed to replace resistance speed as the feedback information of the reference trajectory tracking control strategy.

The differential observer is proposed by the famous scholar Aire Levant. Differential observer technique can accurately estimate the perturbation (see [25,26]). A two order differential sliding mode

* Corresponding author.
E-mail addresses: juandai2011@gmail.com (J. Dai), gaoai@bit.edu.cn (A. Gao), xia_yuanqing@bit.edu.cn (Y. Xia).

http://dx.doi.org/10.1016/j.actaastro.2016.12.013
Received 5 September 2016; Accepted 9 December 2016
Available online 26 December 2016
0094-5765/

observer is proposed for the mechanical system [27]. In [28], a sliding mode controller based on the differential observer is designed to achieve the missile's accurate interception. However, the use of the differential observer to deal with the uncertainty and disturbance of the Mars Lander system is relatively fewer. Moreover, the differential observer is robust and accurate. Therefore, this paper will use the differential observer to deal with the uncertainty and disturbance of the Mars Lander system.

In this paper, the density uncertainty of the Martian atmosphere and the lander gas dynamic uncertain parameters, initial state errors and modeling errors based on non-singular full order terminal sliding mode technique and the differential observer of the Mars Lander atmosphere into the period of robust and high accurate trajectory tracking control problem is discussed. Analysis of the atmospheric into atmospheric density uncertainty, lander gas dynamic uncertain parameters, initial state errors and modeling errors mainly interference effects, design the Mars Lander atmospheric entry trajectory tracking control scheme, the Mars Lander in atmospheric entry the finite time trajectory tracking control. Non-singular full order terminal sliding mode observer to estimate the differential technology and methods, design of anti- interference guidance and control methods compared with the traditional control method of guidance in the aspect of anti-jamming ability is more prominent. The proposed nonlinear compound control law by employing the second-order differentiator provide robustness, higher control precision.

The paper is organized as follows. The Mars entry longitudinal guidance problem is formulated in Section 2. Terminal Sliding Mode Control is presented in Section 3. A novel nonlinear compound controller is presented in Section 4. Simulation results are presented in Section 5 and the paper ends with the conclusion in Section 6.

2. Mars entry guidance problem

The equation of motion of an entry vehicle defined with respect to a planet-fixed coordinate frame are

$$\begin{cases} \dot{\theta} = \frac{V\cos\gamma\sin\psi}{r\cos\phi} \\ \dot{\phi} = \frac{V\cos\gamma\cos\psi}{r} \\ \dot{r} = V\sin\gamma \\ \dot{V} = -D - g\sin\gamma \\ \dot{\gamma} = \frac{1}{V}[L\cos\sigma - (g - \frac{V^2}{r})\cos\gamma] + C_\gamma \\ \dot{\psi} = -\frac{1}{V}[\frac{L\sin\sigma}{\cos\gamma} + \frac{V^2}{r}\cos\gamma\sin\psi\tan\phi] + C_\psi \end{cases} \quad (1)$$

where θ is the longitude, ϕ is the latitude, r is the distance from the center of the planet to the vehicle center of Mars, ψ is the heading angle with $\psi = 0$ as due east, V is the velocity and γ is the flight path angle. L and D are the lift and drag accelerations, defined by

$$L = \frac{1}{2}\frac{\rho S C_L}{m}V^2 \quad (2)$$

$$D = \frac{1}{2}\frac{\rho S C_D}{m}V^2 \quad (3)$$

The drag and lift coefficients C_D and C_L are functions of the Mach number, S is the reference area, m is the lander mass, and ρ is the atmospheric density. The gravity is modeled as $g = \frac{\mu_M}{r^2}$, where μ_M is the Mars gravitational parameter. The term C_γ and C_ψ, are the Coriolis accelerations due to Mars rotation, and given as

$$C_\gamma = 2\omega_p\cos\psi\cos\phi \quad (4)$$

$$C_\psi = 2\omega_p(\tan\gamma\sin\psi\cos\phi - \sin\phi) \quad (5)$$

where ω_p is the planet angular rate. Parameters of the entry vehicle dynamics are referred to (1) and given in Table 1.

The attitude control system uses small thrusters to rotate the vehicle in the path and yaw axes, thus to respond to bank angle commands from the guidance system. The control is the bank angle σ and it is defined such that a positive value corresponds to banking to the right. To account for limits in bank rate (20°/s) and bank acceleration (5°/s^2), a first order bank dynamics controller has been implemented. Commanded bank acceleration is calculated using

$$\dot{\sigma} = \frac{\sigma_c - \sigma}{\tau} \quad (6)$$

where σ is the current bank angle, σ_c is the commanded bank angle and time constant τ of 1 s was chosen for the numerical results in this paper. Then, limits are applied to both commanded bank acceleration and commanded bank rate to obtain the executed bank.

Finally, the cosine of the bank angle is the parameter employed to control the longitudinal motions. The overall goal is to design and test our algorithm that generates a bank angle program that guides the lander to the desired target point during the entry portion of the descent.

Table 1
Parameters of Mars entry vehicle dynamics.

Parameters	r_0 (km)	μ_M (m^3/s^2)	$S(m^2)$	ω_p (rad/s)
Values	3387	4.284	12.8825	7.095e−5
Parameters	C_D (1)	C_L (1)		
Values	1.4595	0.3515		

3. Terminal sliding mode control

Here, the goal is to develop a novel non-linear guidance approach for the Mars entry phase based on the application of recent advancements in TSMC theory (see [29–31]). The overall objective is to derive a guidance law (bank angle program) that is a) robust against parameters uncertainties, and b) guarantees good targeting performances at the end of the entry phase. The guidance model employed to develop the terminal sliding mode guidance algorithm is longitudinal descent model described by Eq. (1).

Let

$$\begin{cases} x_1 = r - r_d \\ x_2 = \dot{r} - \dot{r}_d \end{cases} \quad (7)$$

Here, r_d is the desired distance from the center of the planet to the vehicle center of Mars along the reference trajectory, which are a series of values that are stored as a function of range or range-to-go.

Then, take the derivation of (7), we obtain:

$$\dot{x}_1 = x_2\dot{x}_2 = [-D\sin\gamma - g + \frac{V^2}{r}\cos^2\gamma + V\cos\gamma C_\gamma - \ddot{r}_d] + L\cos\gamma\cos\sigma \quad (8)$$

where, we denote

$$f(x,t) = -D\sin\gamma - g + \frac{V^2}{r}\cos^2\gamma + V\cos\gamma C_\gamma - \ddot{r}_d \, g(x,t) = L\cos\gamma u = \cos\sigma \quad (9)$$

where $x = (\theta, \phi, r, V, \gamma, \psi)$.

Then, we can get

$$\begin{cases} \dot{x}_1 = x_2 \\ \dot{x}_2 = f(x,t) + g(x,t)u \end{cases} \quad (10)$$

The task of Terminal Sliding Mode Control (TSMC) (see [33,34]) for nonlinear system (10) is to design a control strategy which induces an ideal sliding-mode motion in the prescribed sliding-mode surface and forces system (10) to the origin along the sliding-mode surface asymptotically for TSMC. It is assumed that all constants are known, as well as functions $f(x,t)$ and $g(x,t)$ in system (10), and all coordinates are exactly measurable in real time.

A terminal sliding mode variable for system (10) can be selected in the following form, which has been proposed in (see [29]):

$$s = \dot{x}_2 + k_2 sgn(x_2)|x_2|^{\alpha_2} + k_1 sgn(x_1)|x_1|^{\alpha_1} \tag{11}$$

where k_1, k_2 and α_1, α_2 are constants. k_1, k_2 can be selected such that the polynomial $k_1 + k_2 p$, which corresponds to system (10) is Hurwitz, i.e., the eigenvalues of the polynomial are all in the left-half side of the complex plane. α_1, α_2 can be determined based on the following conditions (see [29]):

$$\alpha_2 = \alpha, \quad \alpha_1 = \frac{\alpha}{2-\alpha}, \quad \alpha \in (1-\epsilon, 1), \epsilon \in (0, 1) \tag{12}$$

Once the ideal sliding-mode s=0 is established, the nonlinear system (10) will behave in an identical fashion, namely

$$s = \dot{x}_2 + k_2 sgn(x_2)|x_2|^{\alpha_2} + k_1 sgn(x_1)|x_1|^{\alpha_1} = 0 \tag{13}$$

If α_1, α_2 in terminal sliding mode manifold (13) are selected using (12) and k_1, k_2 in (13) are determined to guarantee that the polynomial $k_1 + k_2 p$ is Hurwitz, which represents the establishment of the ideal sliding-mode s=0 for system (10), can converge to its equilibrium point $x = [x_1, x_2]^T = [0, 0]^T$ from any initial condition $x(0) \neq 0$ along the terminal sliding mode manifold s=0 in finite-time (see [34–37]).

4. Nonlinear compound controller

In this section, we will propose a nonlinear compound controller design for Mars atmosphere entry trajectory tracking control problem. Due to the great advances in nonlinear control theory, the second-order differentiator based controller has become one of the most commonly schemes in industrial applications. The second-order differentiator, which has been developed in (see [25,26]), has the high efficiency in accomplishing the nonlinear dynamic estimation.

Therefore, for solving trajectory tracking problem with Mars atmospheric density uncertainty and lift-to-drag ratio disturbance existing in the lander system, a terminal sliding mode controller can be designed to force the state variables to converge to the reference trajectory by compensating the disturbances via the second-order differentiator.

4.1. Trajectory control concept

Now, consider system (10) containing parameter uncertainty in the form of $\rho = \rho_0 + \Delta\rho$, $L/D = (L/D)_0 + \Delta(L/D)$, and ρ_0, $(L/D)_0$ are the nominal Mars atmospheric density, lift-to-drag ratio, and $\Delta\rho$, $\Delta(L/D)$ denote the Mars atmospheric density uncertainty and lift-to-drag ratio disturbance, respectively. Meanwhile, note that $\Delta(L/D) = \Delta(\frac{\frac{1}{2}\frac{\rho S C_L}{m}V^2}{\frac{1}{2}\frac{\rho S C_D}{m}V^2}) = \Delta(C_L/C_D)$. Then, we can get $C_L = C_{L0} + C_{D0} < MPSAST > \Delta(L/D)$, $C_D = C_{D0} + C_{L0}{}^*\Delta(D/L)$, where C_{D0} and C_{L0} are the nominal drag and lift coefficients.

Hence, notice (2), we can get

$$\begin{cases} \dot{x}_1 = x_2 \\ \dot{x}_2 = \tilde{f}(x, t) + \tilde{g}(x, t)u + \tilde{d} \end{cases} \tag{14}$$

where

$$\tilde{f}(x, t) = \frac{\rho_0 S C_{D0}}{2m} V^2 \sin\gamma - g + \frac{V^2}{r}\cos^2\gamma + V\cos\gamma C_\gamma - \ddot{r}_d \tag{15}$$

$$\tilde{g}(x, t) = \frac{\rho_0 S C_{L0}}{2m} V^2 \cos\gamma \tag{16}$$

$$\tilde{d} = -\frac{SV^2\sin\gamma}{2m}[\Delta\rho C_{D0} + (\rho_0 + \Delta\rho)^* C_{L0}\Delta(D/L)] + \frac{uSV^2\cos\gamma}{2m}[\Delta\rho C_{L0} + (\rho_0 + \Delta\rho)C_{D0}\Delta(L/D)] \tag{17}$$

Thus, we consider the simplified system

$$\begin{cases} \dot{x}_1 = x_2 \\ \dot{x}_2 = \tilde{f}(x, t) + \tilde{g}(x, t)u + \tilde{d} \\ y = x_1 \end{cases} \tag{18}$$

The partially known function $\tilde{d}$, which represents the system parameter uncertainties and the external disturbances, is assumed to satisfy the following condition: $|\tilde{d}| \leq l_d$, where l_d is a bounded constant.

Remark 4.1. It can be seen that if there exists a dynamic state feedback control law such that the solution of the closed-loop system (18) is guaranteed $\lim_{t\to\infty}[x_1(t), x_2(t)] = 0$, Then, the tracking objective can be achieved. Therefore, the reference trajectory tracking problem is solved by the stabilization problem of the nonlinear system (14) which contains both Mars atmospheric density uncertainty and lift-to-drag ratio disturbance.

Remark 4.2. In this section, all the terms are considered sufficiently smooth functions. $\frac{SV^2\sin\gamma}{2m}$, $\frac{uSV^2\cos\gamma}{2m}$ are both differentiable functions. Meanwhile, $\Delta\rho$, $\Delta(L/D)$ are assumed to be differentiable disturbances. In fact, $\Delta\rho$, $\Delta(L/D)$ can be approximated by differentiable functions, when they are not differentiable. Thus, the total disturbances $\tilde{d}$ are differentiable.

4.2. Preliminary

In this subsection, some important definitions and lemmas are presented, which will serve as a basis for this study.

Definition 1. [32] Consider a nonlinear system in the form of

$$\dot{x} = f(x), f(0) = 0, x \in R^n \tag{19}$$

where $f(x)$: $U_0 \to R^n$ is continuous on an open neighborhood U_0 of the origin x=0. The state of system is finite-time convergent to its origin x=0, if for any initial condition $x_0 \in U\backslash\{0\}$, there exists a convergence time $T > 0$, which is dependent on x_0, such that every solution $x(t; x_0) = 0$ of system (19) is defined with $x(t; x_0) = 0 \in U\backslash\{0\}$ for $t \in [0; T)$ and satisfies $\lim_{t\to T(x_0)} x(t, x_0) = 0$ and $x(t, x_0) = 0$, for $t \geq T(x_0)$. Moreover, if the origin x=0 is asymptotically stable and finite-time convergent in a neighborhood of the origin $U \subseteq U_0 \subset R^n$, then the origin x=0 of the system is (locally) finite-time stable. If $U = R^n$, system (19) is globally finite-time stable.

Assumption 1. The derivative of $\tilde{d}$ in system (18) is bounded:

$$|\dot{\tilde{d}}| \leq k_d \tag{20}$$

where $k_d > 0$ is a constant.

Lemma 1. [32] Consider the nonlinear system described by Eq. (19). Suppose that there is a continuously differentiable function $V(x)$: $U \to R$, and that there are real numbers $k > 0$ and $0 < a < 1$ and an open neighborhood $U_0 \subset U$ of the origin such that $V(x)$ is positive definite on U_0 and that $\dot{V}(x) \leq -kV^a(x)$, $x \in U_0\backslash\{0\}$. Then, the origin x=0 of system (19) is finite-time stable. Moreover, if T is the convergence time, then $T(x) \leq \frac{1}{k(1-a)}V^{1-a}(x(0))$ for all $x(0)$ in some open neighborhood of the origin. If $U = U_0 = R^n$, the origin x=0 of system (19) is globally finite-time stable.

Lemma 2. [33] (Input-to-State Stability Theorem, ISS Theorem) Consider the following nonlinear system

$$\dot{x} = f(x, u, t) \tag{21}$$

If the system $\dot{x} = f(x, 0, t)$ is globally uniformly asymptotically stable, and $\lim_{t\to\infty} u = 0$, then the states of system (21) are asymptotically convergent to zero, i.e., $\lim_{t\to\infty} x = 0$.

Lemma 3. [25] Considering the closed-loop system (18) and the formula (13), when $\tilde{f}$ and $\tilde{g}$ are sufficiently smooth functions, and $\tilde{d}$ are differentiable, the second-order differentiator proposed for the estimate of the total disturbance $\tilde{d}$ take the form

$$\dot{z}_0 = \widetilde{f} + \widetilde{g}u + v_0 v_0 = -\lambda_0 K^{\frac{1}{3}}|z_0 - \dot{y}|^{\frac{2}{3}} sign(z_0 - \dot{y}) + z_1 \dot{z}_1 = v_1 v_1 = -\lambda_1 K^{\frac{1}{2}} |z_1 - v_0|^{\frac{1}{2}} sign(z_1 - v_0) + z_2 \dot{z}_2 = -\lambda_2 K sign(z_2 - v_1) \quad (22)$$

where z_0, z_1 and z_2 are the estimate of $\dot{y}$, $\widetilde{d}$ and $\dot{\widetilde{d}}$, respectively; $K \geq |\ddot{\widetilde{d}}|$.

4.3. Controller design

With the disturbances of system $\widetilde{d}$ estimated by the second-order differentiator, using the TSMC algorithm, the proposed nonlinear controller for low lift landers system (18) can be design as

$$u_D = \widetilde{g}(x, t)^{-1}(u_1 + u_2) u_1 = -z_1 - \widetilde{f}(x, t) - k_2 sgn(x_2)|x_2|^{\alpha_2} - k_1 sgn(x_1)|x_1|^{\alpha_1} \dot{u}_2 + T u_2 = \nu\nu = -(k_d + k_T + \eta) sgn(s) \quad (23)$$

where u_D is the design controller of this paper; $u(0) = 0$; k_1, k_2 and α_1, α_2 are all constants, as defined in (13); k_d is a constant defined in (20), T, η are positive constants, k_T are selected satisfy the following condition:$k_T \geq T l_d$.

Remark 4.3. Note that the second formula z_1 in (22) is most important. It shows that z_1 can estimate (or track) the total action of the uncertain models and the external disturbances or the real-time action of the system disturbances. As z_1 is the estimation for the total action of the unknown disturbances, in the feedback, z_1 is used to compensate for the disturbances.

In this subsection, the stability of the system (18) can be established by the following theorem.

Theorem 1. Consider the system (18), control law (23), second-order differentiator (22), there exist gains λ_0, λ_1, λ_2, such that the estimated states z_0, z_1, z_2 converge into a residual set of the actual states $\dot{y}$, $\widetilde{d}$, $\dot{\widetilde{d}}$ respectively, and the trajectory of the closed-loop system can be driven onto the sliding surface in a finite time and finally converges to the origin.

Proof. In order to examine stability of the system (18), one must develop an expression for the second-order differentiator error dynamic. Defining the second-order differentiator error

$$\begin{cases} e_1 = z_0 - \dot{y} \\ e_2 = z_1 - \widetilde{d} \\ e_3 = z_2 - \dot{\widetilde{d}} \end{cases} \quad (24)$$

□The second-order differentiator error dynamic are expressed as

$$\dot{e}_1 = \dot{z}_0 - \ddot{y} = v_0 - \dot{\widetilde{d}} = -\lambda_0 K^{\frac{1}{3}}|z_0 - \dot{y}|^{\frac{2}{3}} sign(z_0 - \dot{y}) + z_1 - \dot{\widetilde{d}} = -\lambda_0 K^{\frac{1}{3}}|e_1|^{\frac{2}{3}} sign(e_1) + e_2 \quad (25)$$

$$\dot{e}_2 = \dot{z}_1 - \ddot{\widetilde{d}} = v_1 - \ddot{\widetilde{d}} = -\lambda_1 K^{\frac{1}{2}}|e_2 - \dot{e}_1|^{\frac{1}{2}} sign(e_2 - \dot{e}_1) + e_3 \quad (26)$$

$$\dot{e}_3 = \dot{z}_2 - \dddot{\widetilde{d}} = -\lambda_2 K sign(e_3 - \dot{e}_2) - \dddot{\widetilde{d}} \quad (27)$$

The stability of second-order differentiator has been obtained by selecting appropriate parameters λ_0, λ_1, λ_2, and K. According to Lemma 3, z_0, z_1 and z_2 are the real time estimates of $\dot{y}$, $\widetilde{d}$, $\dot{\widetilde{d}}$. When the observer is stable, the derivative of vector $[\dot{e}_1, \dot{e}_2, \dot{e}_3]^T = 0$.

Having shown that the second-order differentiator error converges into the residual set of zero, it remains to shown that the system states converge to the origin in finite time.

Considering the Lyapunov function candidate with the terminal sliding surface given by (13), the second-order differentiator obtained by (22), we obtain

$$s = \dot{x}_2 + k_2 sgn(x_2)|x_2|^{\alpha_2} + k_1 sgn(x_1)|x_1|^{\alpha_1} = \widetilde{f}(x, t) + \widetilde{g}(x, t)u + k_2 sgn(x_2)|x_2|^{\alpha_2} + k_1 sgn(x_1)|x_1|^{\alpha_1} = \widetilde{f}(x, t) + u_1 + u_2 + k_2 sgn(x_2)|x_2|^{\alpha_2} + k_1 sgn(x_1)|x_1|^{\alpha_1} = \widetilde{d} - z_1 + u_2 = -e_2 + u_2 \quad (28)$$

From (28) and (13), we can get

$$s = -e_2 + u_2 = 0 \quad (29)$$

In addition, the solution of (23) is given by

$$u_2 = [u_2(t_0) + \frac{k_T + k_d + \eta}{T} sgn(s)] e^{T(t_0 - t)} - \frac{k_T + k_d + \eta}{T} sgn(s) \quad (30)$$

From (23) and (30), the following relationship under the condition $u_2(0) = 0$ can be obtained:

$$|u_2(t)| \leq |u_2(t)|_{max} \leq k_T / T \quad (31)$$

i.e. the following inequality will be kept forever:

$$T|u_2(t)| \leq k_T \quad (32)$$

The following Lyapunov function is considered:

$$V = \frac{s^2}{2}$$

For terminal sliding mode manifold (13), its derivative with respect to time t along system (10) can be obtained from (28) as follows:

$$\dot{s} = -\dot{e}_2 + \dot{u}_2 = -\dot{e}_2 - T u_2 + \nu = -\dot{e}_2 - T u_2 - (k_T + k_d + \eta) sgn(s) \quad (33)$$

Hence,

$$\dot{V} = s\dot{s} = s(-\dot{e}_2 - T u_2 - (k_T + k_d + \eta) sgn(s)) = s(-\dot{e}_2 - T u_2 - (k_T + k_d + \eta) sgn(s)) = -(k_d |s| + s\dot{e}_2) - (T u_2 s + k_T |s|) - \eta |s| \leq -\eta |s| = -\eta V^{\frac{1}{2}} \quad (34)$$

It has been shown that the second-order differentiator is stable and $z_2(t)$ converges into a residual set of $\widetilde{d}$, which means $\dot{e}_2$ converges into a residual set of zero.

Appropriate T, k_d, k_T, η can be selected such that $\dot{V} < 0$, when V is out of a certain bounded region which contains equilibrium point. Thus, it can be concluded that with the bounded motion around the sliding surface, the state x of system (18) will converge into a neighborhood of the origin, which implies state x is uniformly ultimately bounded.

Remark 4.4. The system (18) can be made to converge using Terminal sliding mode control methods [29]. However, in order to suppress the uncertainty and disturbance, the control input may lead to violent chattering which is normally undesirable in practice. Hence, the second-order differentiator can be adopted here to make the total disturbance estimated and compensated in the control input, which implies the decrease of the chattering and control power.

Remark 4.5. Since the second-order differentiator cannot track the signal completely in any practical systems, asymptotic stability is lost and it can only guarantee the bounded motion about the sliding surface. Therefore, we cannot analyze the stability of the dynamics of the sliding mode that is restricted on the sliding surface. In (34) the boundary layer of sliding surface is affected by the estimation error of the second-order differentiator. Thus the parameter selecting of the second-order differentiator is more important, since it not only determines the performance of second-order differentiator estimating the total disturbances, but also impacts the behavior of sliding surface. More information about the parameter selecting for the second-order differentiator can been seen in (see [25,26]) .

5. Simulation results

5.1. Numerical values of tracking control

In this paper, the model presented is based on the model of the described in [20]: 1) a spherical gravitational field that accounts for Mars non-flat surface; 2) a first order bank angle autopilot model that models the dynamics as: $\dot{\sigma} = \frac{\sigma_c - \sigma}{\tau}$. A time constant τ of 1 s was chosen for these runs; 3) A Martian atmosphere as described by [2] was used to compute the lift and drag accelerations as function of altitude and velocity. Three cases of the atmospheric density disturbances are considered. Case 1: $\Delta\rho = +30\%$; Case 2: $\Delta\rho = +50\%$; Case 3:

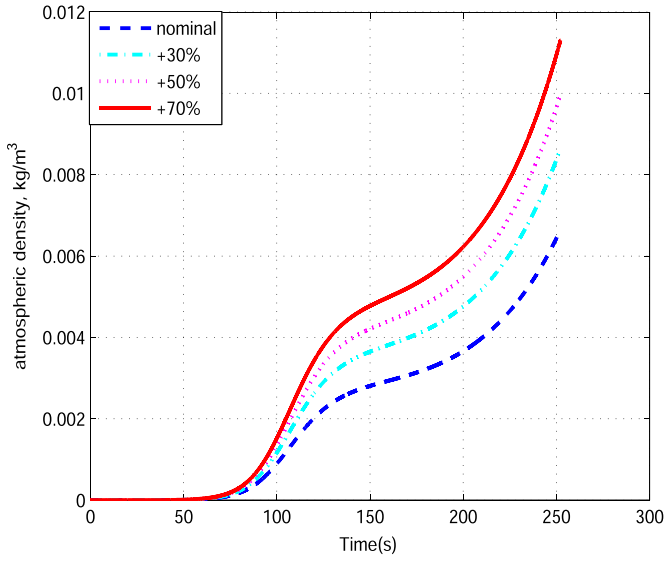

Fig. 1. Martian atmospheric density.

$\Delta\rho = +70\%$. The Martian atmospheric density disturbances are shown in Fig. 1.

The reference trajectory was created by running a nominal simulation at a constant bank angle of 59.63° with the velocity heading not allowed to change. This is similar to the method used by [38]. The simulation is stopped once the lander reaches its desired altitude.

To evaluate the robustness of the proposed algorithm (23), a 1000-run Monte Carlo study has been performed. The set of initial conditions and guidance parameters that do not change from run to run for these Monte Carlo runs are shown in Table 2. In this set of Monte Carlo simulations, the parameters taken to perform the simulation come largely from the MSL landers data.

As mentioned above, the entry guidance task is to deliver the lander to the desire parachute deployment point, thus a termination logic of the simulated entry should be proposed. According to the requirement of the high landing altitude, hence, the parachute is deployed when the altitude range 8.1–12 km, and the velocity of the vehicle is less than 450 m/s. Otherwise, when the altitude h=8.1 km, or the velocity V=450 m/s, the parachute is deployed, whichever takes place first.

A 1000-run Monte Carlo study was performed to evaluate the robustness of the proposed method in presence of the dispersions in entry state and model errors. The drag and lift coefficients dispersions are modeled as random Gaussian distributions as well as the entry state dispersion, and their dispersions are ±30%. Whereas, the density dispersion is modeled as random multiplier factors, and the density dispersion is ±40%. The means and the standard deviations for the initial state variables are shown in Table 3.

5.2. Comparisons results of two controllers

To make a fair comparison of the control performances(e.g. high-precision and strong robustness), we consider the proposed control law u_D and [29] in the same Case 1.

The comparison results are shown in Figs. 2–9. And Figs. 2 and 3 show the reference and actual tracking states. Figs. 4 and 5 show trajectory tracking errors between the current trajectory and the reference trajectory. Figs. 6–9 show the results of the 1000-run Monte Carlo analysis. The stopping condition for all runs is implemented whenever the lander reaches an altitude of 8.1 km. Figs. 8 and 9 show the lading dispersion. It can be seen in the 99.8% of the runs, three standard deviations from the mean, are under 10 km residual error in Fig. 8. However, it can be seen in the only 18% of the runs, three standard deviations from the mean, are under 10 km residual

Table 2
Simulation conditions and parameters.

Parameters	θ_i (deg)	ϕ_i (deg)	h_i (km)	V_i (m/s)
Initial Values	−90.072	−43.898	133.56	5505
Parameters	γ_i (deg)	ψ_i(deg)		
Initial Values	−14.15	4.99		
Parameters	θ_t(deg)	ϕ_t (deg)	h_t (km)	V_t(m/s)
Target Values	−73.26	−41.43	8.10	450

Table 3
Dispersion parameters used in the Monte Carlo Simulations.

Parameters	θ_i (deg)	ϕ_i (deg)	h_i (km)
Initial Values	−90.072	−43.898	133.56
3 var	0.15	0.03	2.306
Parameters	V_i (m/s)	γ_i (deg)	ψ_i(deg)
Initial Values	5505	−14.15	4.99
3 var	2.85	0.15	0.23
Parameters	ρ	L/D	
Values	Sehnal Mars Atmosphere profile	0.24	
3 var	13.3%	0.03	

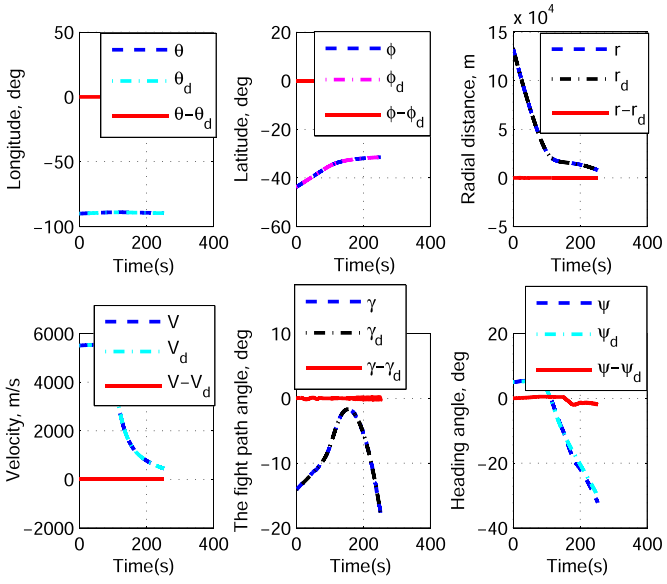

Fig. 2. Reference and actual tracking states: u_D.

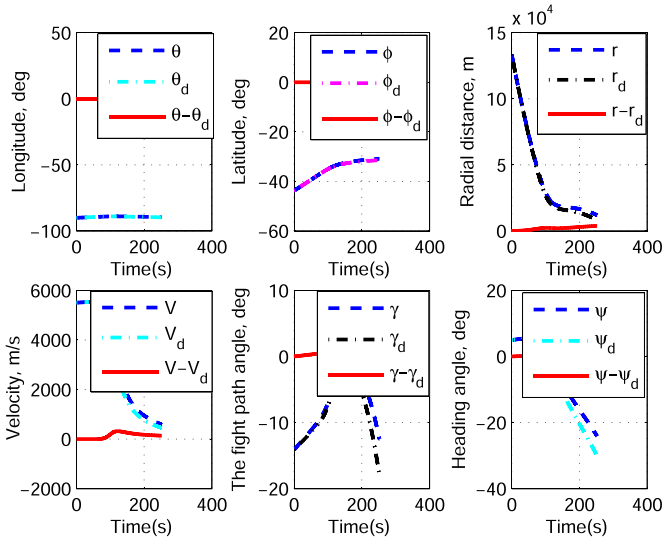

Fig. 3. Reference and actual tracking states: [29].

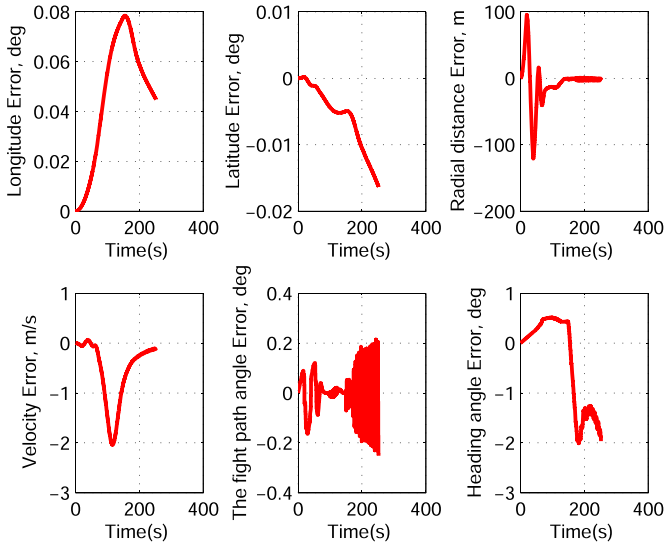

Fig. 4. Trajectory tracking errors: u_D.

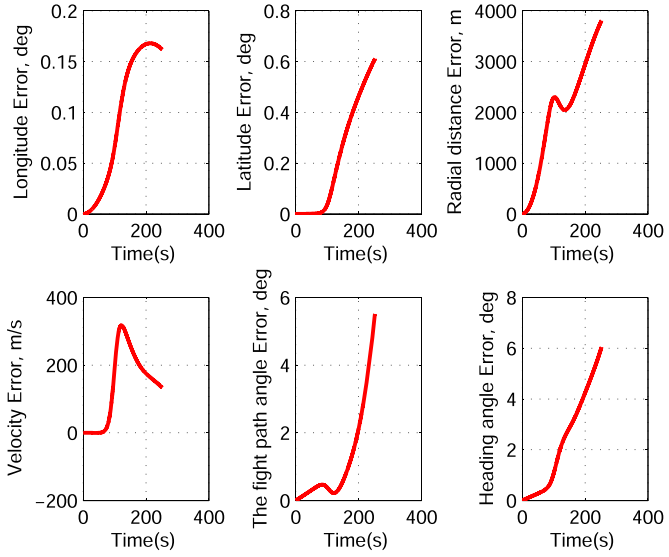

Fig. 5. Trajectory tracking errors: [29].

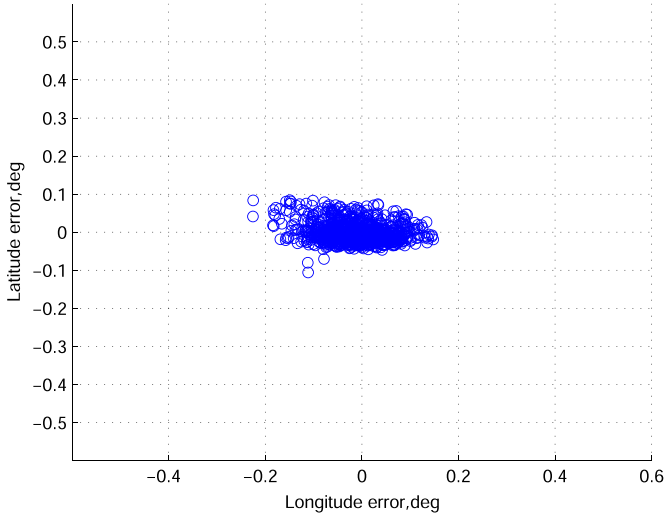

Fig. 6. Latitude and Longitude errors: u_D.

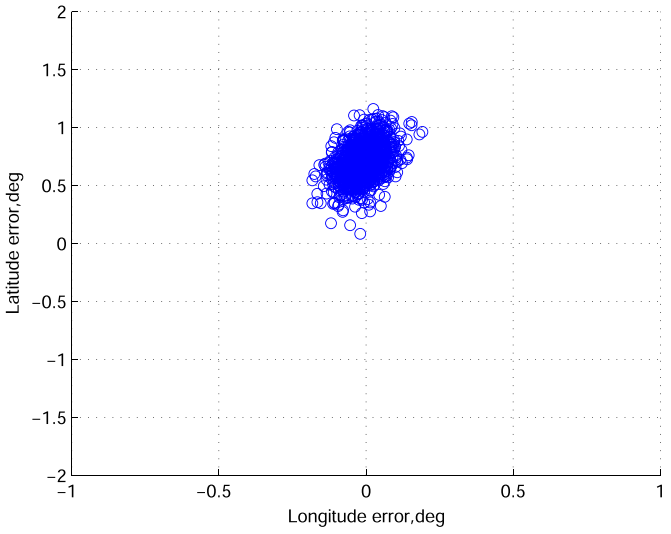

Fig. 7. Latitude and Longitude errors: [29].

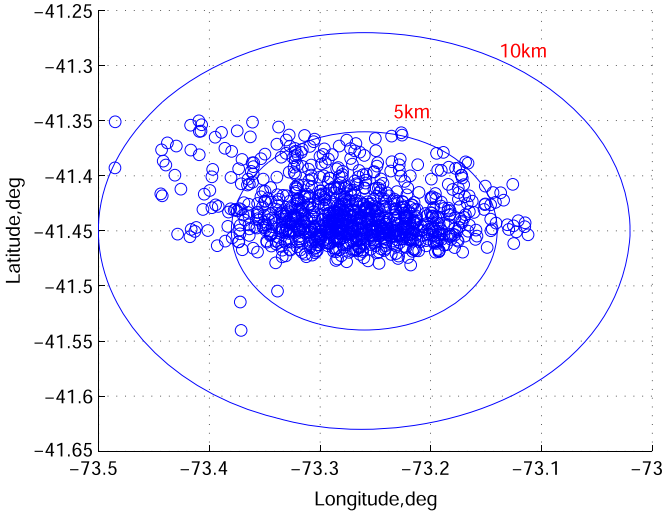

Fig. 8. Lander dispersion with 5 km and 10 km landing dispersion ellipse for 1000 Monte Carlo runs: u_D.

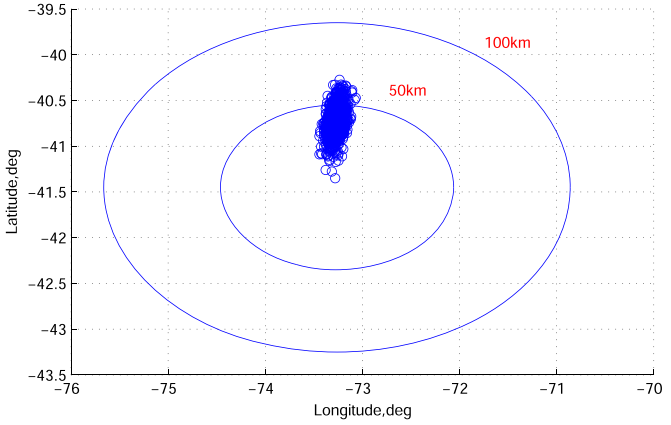

Fig. 9. Lander dispersion with 50 km and 100 km landing dispersion ellipse for 1000 Monte Carlo runs: [29].

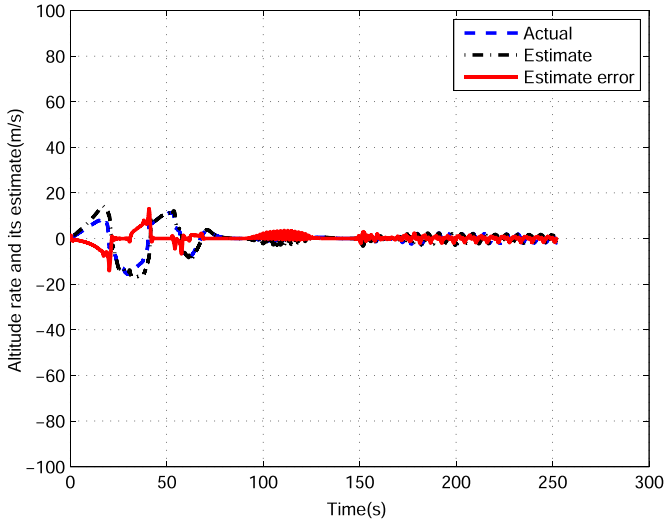

Fig. 10. Altitude rate and its estimate: u_D.

error in Fig. 9.

It is observed that the proposed control law (23) provides superior control performance than this in [29] in both theory and simulations. The proposed controller schemes u_D based on an optimized dynamic equation $\tilde{d}$ can provide faster, higher tracking control precision than those in [29] (see Fig. 6–9).

Based on Figs. 4, 6, 8, the proposed control laws (23) are able to achieve more accurate tracking in spite of Mars atmospheric density uncertainty and lift-to-drag ratio disturbance existing in the Mars Atmospheric Entry system. In addition, extensive simulations are also done using different disturbances in Case 2 and Case 3. .

5.3. Comparisons results of various disturbances and values

In this section, simulation values of the Case 2 and Case 3 are considered to the robustness of the proposed control law. Figs. 11–18 show the results of the trajectory tracking under the sliding mode control (see [29]) based on the second-order differentiator with Mars atmospheric density uncertainty and lift-to-drag ratio disturbance existing in the spacecraft system in Case 2 and Case 3. Figs. 11 and 12 show the trajectory tracking errors between the current trajectory and the reference trajectory. Figs. 13 and 14 show trajectory tracking errors between the current trajectory and the reference trajectory. Figs. 15–18 show the results of the 1000-run Monte Carlo analysis. The stopping condition for all runs is implemented whenever the lander reaches an altitude of 8.1 km. Figs. 17 and 18 show the lading

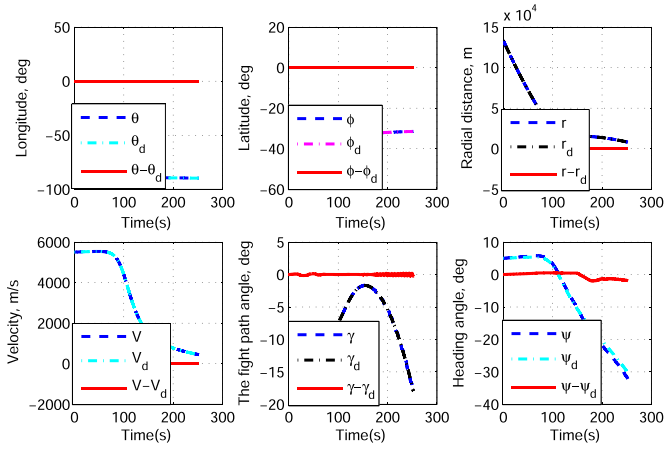

Fig. 11. Reference and actual tracking states: Case2.

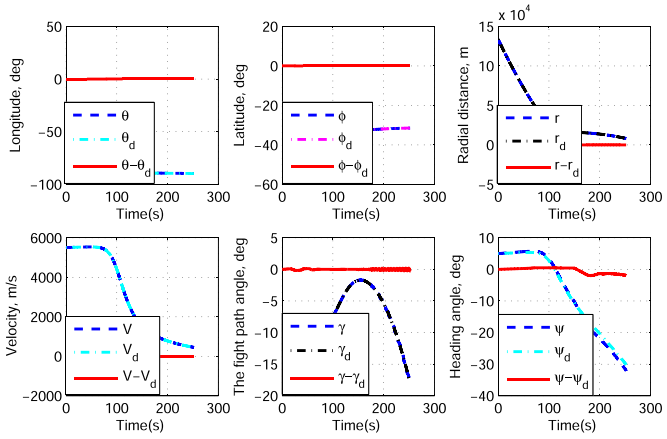

Fig. 12. Reference and actual tracking states: Case3.

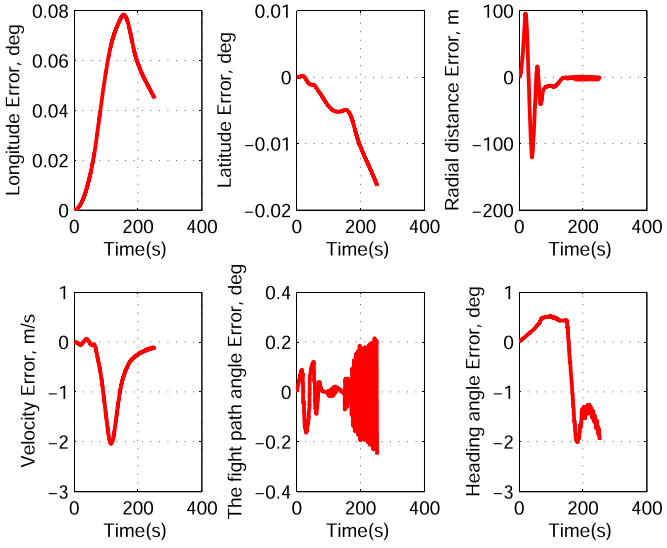

Fig. 13. Trajectory tracking errors: Case2.

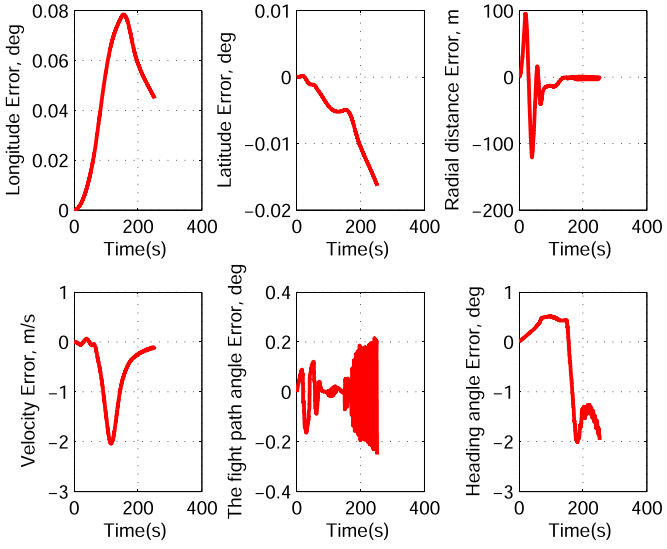

Fig. 14. Trajectory tracking errors: Case3.

dispersion.

The simulation results of controller (23) in Case 2 and Case 3 are depicted in Figs. 17 and 18, respectively. The control performances under different disturbances are shown in Figs. 17, 18. Compared to in

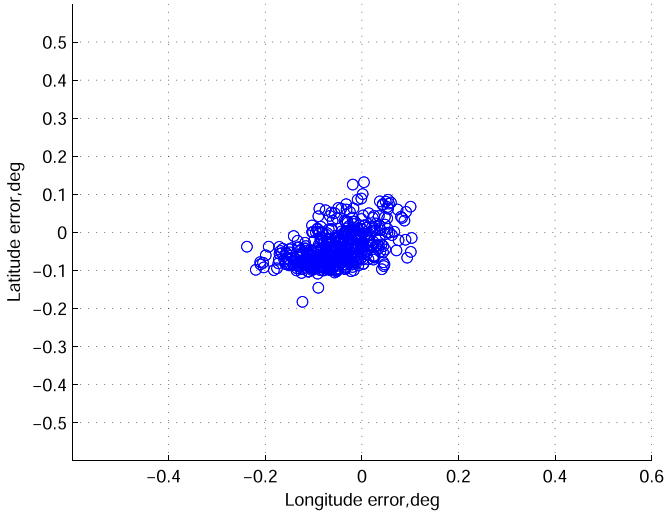

Fig. 15. Latitude and Longitude errors: Case2.

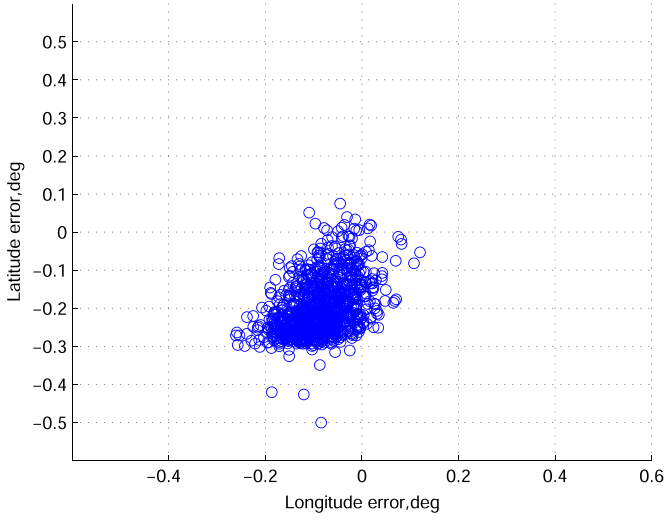

Fig. 16. Latitude and Longitude errors: Case3.

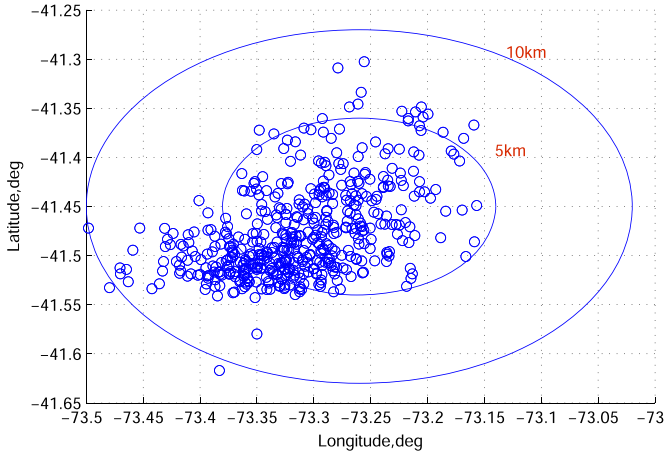

Fig. 17. Lander dispersion with 5 km and 10 km landing dispersion ellipse for 1000 Monte Carlo runs: Case2.

Case 3, the proposed controller (23) can provide a more accurate dispersion in Case 2.

From above comparison, it is obvious that the novel proposed control law u_D can achieve faster and more accurate tracking performance in the presence of Mars atmospheric density uncertainty and lift-to-drag ratio disturbance than this in (see [29]) (see Figs. 8, 17, 18 and 9).

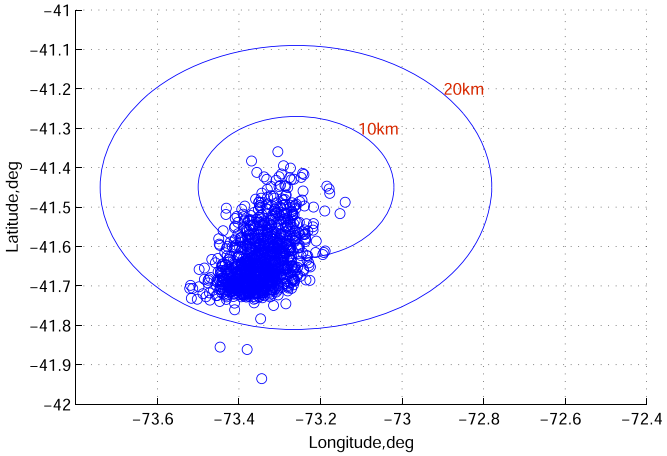

Fig. 18. Lander dispersion with 10 km and 20 km landing dispersion ellipse for 1000 Monte Carlo runs: Case 3.

Based on Fig. 4–18, the control laws (23) are able to achieve more accurate tracking in spite of Mars atmospheric density uncertainty and lift-to-drag ratio disturbance existing in the Mars Atmospheric Entry system.

In order to demonstrate effectiveness of the proposed controller (23), we do not change any parameter except the total uncertainties $\tilde{d}$ being replaced by z_1. When the atmospheric density changes, the proposed control law (23) can also provide better control ability than [29]. Although the atmospheric density disturbances is large, the Lander dispersion of controller (23) in Case 2 and Case 3 is also reduced effectively (see Fig. 17, Figs. 18 and 9), which means controller (23) can provide high control performance(e.g. faster, higher tracking control precision) although the large atmospheric density disturbances, and the designed method of proposed control laws (23) is more effective.

6. Conclusion

In this paper, the trajectory tracking control problem of the Mars atmospheric entry guidance with Mars atmospheric density uncertainty and lift-to-drag ratio disturbance existing in the spacecraft system has been studied using TSMC associated with the second-order differentiator. The second-order differentiator is applied to estimate the total disturbances of system, which has the high efficiency in accomplishing the nonlinear dynamic estimation, by which terminal sliding mode controllers are designed combing the two approaches respectively to force the state variables of the closed-loop system to converge to the reference trajectory. The proposed terminal sliding mode control law by employing second-order differentiator provide finite-time convergence, robustness, higher control precision. Meanwhile, the analysis of the statistical results of the Monte Carlo runs shows that the proposed algorithm performs well under perturbations and make is suitable for real-time implementation.

Acknowledgements

The authors would like to thank the reviewers for their very helpful comments and suggestions which have improved the presentation of the paper. This work is supported by National Basic Research Program of China (973 Program) (2012CB720000), the National Natural Science Foundation of China (61225015, 61304226, 61105092, 61422102), the Beijing Natural Science Foundation (4161001), Foundation for Innovative Research Groups of the National Natural Science Foundation of China (61321002).

References

[1] R. Shotwell, Phoenix-the first Mars Scout mission, Acta Astronaut. 57 (2005) 121–134.
[2] C.D. Karlgaard, P. Kutty, M. Schoenenberger, J. Shidner, M. Munk, Mars entry atmospheric data system trajectory reconstruction algorithms and flight results, in: Proceedings of the 51st AIAA Aerospace Sciences Meeting Including the New Horizons Forum and Aerospace Exposition, Paper no. 2013–0028, 2013.
[3] A. Lele, Mission Mars. Springer Briefs in Applied Sciences and Technology, India: Springer
[4] A. Chen, A. Vasavada, A. Cianciolo, J. Barnes, D. Tyler, S. Rafkin, Atmospheric risk assessment for the Mars science laboratory entry, descent, and landing system, in: Proceedings of IEEE Aerospace Conference, 2010.
[5] A.D. Steltzner, D.M. Kipp, A. Chen, P.D. Burkhart, C.S. Guernsey, G.F. Mendeck, R. A. Mitcheltree, R.W. Powell, T.P. Rivellini, A.M. San Martin, D.W. Way, Mars science laboratory entry, descent, and landing system, in: Proceedings of IEEE Aerospace Conference, Paper No. 2006–1497, 2006.
[6] M.J. Grant, B.A. Steinfeldt, R.D. Braun, G.H. Barton, Smart divert: a new Mars robotic entry, descent, and landing architecture, Spacecr. Rockets 47 (4) (2010) 385–393.
[7] G.F. Mendeck, G.L. Carman, Guidance design for mars smart landers using the entry terminal point controller, AIAA, Paper No. 2002–4502, 2002.
[8] K.Y. Tu, M.S. Munir, K.D. K.D. Mease, D.S. Bayard, Drag-based predictive tracking guidance for mars precision landing, J. Guid., Control, Dyn. 23 (4) (2000) 620–628.
[9] P. Lu, Predictor-corrector entry guidance for low lifting vehicles, J. Guid., Control, Dyn. 31 (4) (2008) 1067–1075.
[10] Y. Xia, G. Shen, L. Zhou, H. Sun, Mars entry guidance based on segmented guidance predictor-corrector algorithm, Control Eng. Pract. 45 (2015) 79–85.
[11] A. Halder, R. Bhattacharya, Dispersion analysis in hypersonic flight during planetary entry using stochastic Liouville equation, J. Guid., Control, Dyn. 34 (2) (2011) 459–474.
[12] J.F. Levesque, Advanced navigation and guidance for high-precision planetary landing on Mars. 2006.
[13] P.D. Burkhart, J. Casoliva, MSL DSENDS EDL analysis and operations, in: Proceedings of the 23rd International Symposium on Space Flight Dynamics, 2012.
[14] I.G. Clark, A.L. Hutchings, C.L. Tanner, et al., Supersonic inflatable aerodynamic decelerators for use on future robotic missions to Mars, J. Spacecr. Rockets 46 (2) (2009) 340–352.
[15] Z. Zhao, J. Yang, S. Li, Z. Zhang, L. Guo, Finite-time super-twisting sliding mode control for Mars entry trajectory tracking, J. Frankl. Inst. 352 (11) (2015) 5226–5248.
[16] S. Li, Y. Peng, Command generator tracker based direct model reference adaptive tracking guidance for Mars atmospheric entry, Adv. Space Res. 49 (1) (2012) 49–63.
[17] S. Li, Y. Peng, Neural network-based sliding mode variable structure control for Mars entry, Proc. Inst. Mech. Eng., Part G: J. Aerosp. Eng. 226 (11) (2012) 1373–1386.
[18] S. Li, X. Jiang, Review and prospect of guidance and control for Mars atmospheric entry, Prog. Aerosp. Sci. 69 (2014) 40–57.
[19] S.E. Talole, J. Benito, K.D. Mease, Sliding mode observer for drag tracking in entry guidance, Proceedings of the AIAA Guidance, Navigation and Control Conference, Paper No. 5122–5137, 2007.
[20] R. Furfaro, D.R. Wibben, Mars atmospheric entry guidance via multiple sliding surface guidance for reference trajectory tracking, AIAA, Paper No. 2012–4435, 2012.
[21] B. Tian, Q. Zong, Optimal guidance for reentry vehicles based on indirect Legendre pseudospectral method, Acta Astronaut. 68 (7) (2011) 1176–1184.
[22] A.M. Korzun, G.F. Dubos, C.K. Iwata, et al., A concept for the entry, descent, and landing of high-mass payloads at Mars, Acta Astronaut. 66 (7) (2010) 1146–1159.
[23] Y. Wang, D. Qiao, P. Cui, Analysis of two-impulse capture trajectories into Halo orbits of Sun-Mars system, J. Guid., Control, Dyn. 37 (3) (2014) 985–990.
[24] E. Garcia-Llama, M.C. Ivanov, R.G. Winski, et al., Mars Science Laboratory entry guidance improvements study for the Mars 2018 mission, in: Proceedings of Aerospace Conference, Paper No. 1-11, 2012.
[25] A. Levant, Higher-order sliding modes, differentiation and output feedback control, Int. J. Control 76 (9) (2003) 924–941.
[26] A. Levant, Principles of 2-sliding mode design, Automatica 43 (4) (2007) 576–586.
[27] J. Davila, L. Fridman, A. Levant, Second-order sliding-mode observer for mechanical systems, IEEE Trans. Autom. Control 50 (11) (2005) 1785–1789.
[28] Y.B. Shtessel, I. Shkolnikov, A. Levant, Guidance and control of missile interceptor using second-order sliding modes, IEEE Trans. Aerosp. Electron. Syst. 45 (1) (2009) 110–124.
[29] Y. Feng, F.L. Han, X.H. Yu, Chattering free full-order sliding-mode control, Automatica 50 (4) (2014) 1310–1314.
[30] S.H. Ding, S.H. Li, Stabilization of the attitude of a rigid spacecraft with external disturbances using finite-time control techniques, Aerosp. Sci. Technol. 13 (4) (2009) 256–265.
[31] E.D. Jin, Z.W. Sun, Robust controllers design with finite time convergence for rigid spacecraft attitude tracking control, Aerosp. Sci. Technol. 12 (4) (2008) 324–330.
[32] S.P. Bhat, D.S. Bernstein, Finite-time stability of continuous autonomous systems, SIAM J. Control Optim. 38 (3) (2000) 751–766.
[33] Y.G. Hong, J. Huang, Y.S. Xu, On an output feedback finite-time stabilization problem, IEEE Trans. Autom. Control 46 (2) (2001) 305–309.
[34] S.P. Bhat, D.S. Bernstein, Geometric homogeneity with applications to finite-time stability, Math. Control, Signals Syst. 17 (2) (2005) 101–127.
[35] Y.G. Hong, Y.S. Xu, J. Huang, Finite-time control for robot manipulators, Syst. Control Lett. 46 (4) (2002) 243–253.
[36] Y.G. Hong, G. Yang, D. Cheng, S. Spurgeon, Finite time convergent control using terminal sliding mode, J. Control Theory Appl. 2 (1) (2004) 69–74.
[37] Y.C. Huang, H.Y. Li, J. Zhang, X. Du, Mars atmospheric entry guidance design by sliding mode disturbance observer-based control, Procedia Eng. 99 (2004) 1062–1075.
[38] C.A. Kluever, Entry guidance performance for Mars precisions landing, J. Guid., Control, Dyn. 31 (6) (2008) 1537–1544.